

# Direct Evidence in the Scattering Function for the Coexistence of Two Types of Local Structures in Liquid Water

Rui Shi and Hajime Tanaka\*



Cite This: *J. Am. Chem. Soc.* 2020, 142, 2868–2875



Read Online

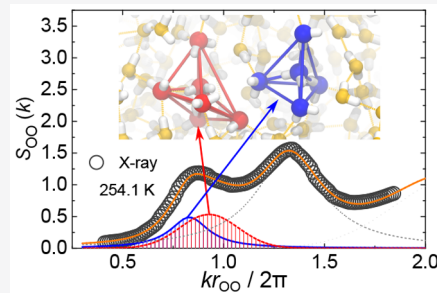
ACCESS |

Metrics & More

Article Recommendations

Supporting Information

**ABSTRACT:** Water is the essential liquid on earth since it not only plays vital roles in living systems but also has a significant impact on our daily life from various industrial applications to earth's climate system. However, the unusual properties of liquid water, if compared with other liquids, has puzzled us for centuries because the basic structure of liquid water has remained unclear and has continued to be a matter of serious debate. Here, by computer simulations of three popular water models and the analysis of recent scattering experimental data, we show that there are two overlapped peaks hidden in the apparent "first diffraction peak" of the structure factor. One of them (ordinary peak) corresponds to the neighboring O–O distance as in ordinary liquids, and the other (anomalous peak) corresponds to a longer distance. We reveal that this anomalous peak arises from the most extended period of density wave associated with a tetrahedral water structure and is to be identified as the so-called first sharp diffraction peak that is commonly observed in silica and other tetrahedral liquids. In contrast, the ordinary peak arises from the density wave characteristic of local structures lacking tetrahedral symmetry. This finding unambiguously proves the coexistence of two types of local structures in liquid water. Our findings not only provide vital clues to settle a long-standing controversy on the water structure but also allow direct experimental access to the fraction of tetrahedral structures in liquid water.



## INTRODUCTION

Water is ubiquitous on our planet and plays vital roles in many biological, geological, meteorological, and technological processes. Despite its simple molecular structure, water has many unique thermodynamic and dynamic properties in the liquid state, such as a density maximum at 4 °C, a rapid increase in isothermal compressibility,<sup>1</sup> and a dynamic fragile-to-strong transition<sup>2,3</sup> upon cooling.<sup>4–6</sup> These unusual properties, which are absent in ordinary liquids, are well known as "water's anomalies". It is widely believed that the anomalies are linked to water's structural ordering toward tetrahedral structures stabilized by four hydrogen bonds (H-bonds). Even after intensive studies for more than a century, how such structural ordering takes place is still a matter of hot debate without convergence.

Two conflicting different scenarios have continued to exist until now: continuum models based on a broad unimodal distribution of structural components and mixture models based on a bimodal (or multimodal) distribution of structural components reflecting the coexistence of two (or more) types of local structures.<sup>7–9</sup> The mixture model dates back to Wilhelm Röntgen, who proposed in 1892 that water can be regarded as a mixture of "icebergs" and a fluid "sea".<sup>10</sup> Later, various mixture models were developed. One famous example is the mixture model of Linus Pauling, who proposed in 1959 that water is a mixture of clathrate-like structure and interstitial molecules.<sup>11</sup> These mixture models, however, have been continuously challenged by the continuum model dating

back to John Pople, who proposed in 1951 that water's structure can be described by a continuously distorted H-bond network.<sup>12</sup>

These two types of models lead to fundamentally different understandings of water structure. Despite such a clear difference in the physical picture, this debate has never converged for a century. The main reason is the lack of experimental evidence exclusively supporting either of the models. In this article, we provide clear evidence that liquid water is indeed a mixture of two types of local structures, from simulations of three popular water models and detailed analysis of recent scattering experiments.

## RESULTS AND DISCUSSION

**Five Features of Our Two-State Model.** First, we need to explain the precise nature of our two-state model to clarify essential differences from continuum models. The following five features characterize our two-state model that regards water as a mixture of ordered (*S*) and less ordered local structures (*ρ* state):<sup>13–15</sup> (1) *S* and *ρ* states in liquid water are

Received: October 18, 2019

Published: January 21, 2020

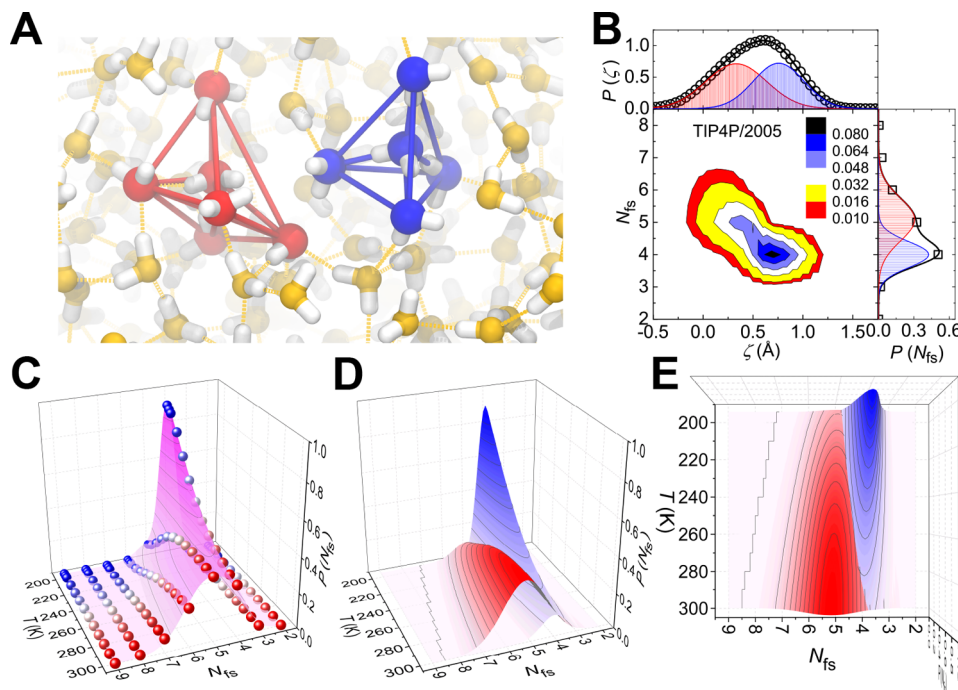


**Figure 1.** Structural bimodality in the coordination number distribution of liquid water. (A) Snapshot of liquid TIP4P/2005 water at 1 bar and 240 K, where  $s \approx 0.5$ , i.e., near the Schottky temperature,  $T_{s=1/2}$ . Two types of local structures, LFTS and DNLS, are highlighted by blue and red colors, respectively. LFTS has four H-bonded nearest neighbors with tetrahedral coordination, whereas DNLS typically has five or more nearest neighbors (typically three of them being H-bonded) with broken tetrahedral symmetry. (B) Correlation between the number of water molecules in the spherical first-shell volume of radius of 3.5 Å,  $N_{fs}$ , i.e., the coordination number, and structural descriptor  $\zeta$  in TIPSP/2005 water at 1 bar and 240 K. The distributions of  $N_{fs}$  and  $\zeta$  are shown in the right and top panels, respectively. Both distributions show clear bimodal features, which can be properly described by the sum of two Gaussian functions (black lines), with blue and red shades corresponding to LFTS and DNLS, respectively. (C) Distribution of coordination number  $N_{fs}$  as a function of temperature,  $P(N_{fs}, T)$ , in TIPSP/2005 water shown by colored balls with red and blue for higher and lower temperatures, respectively. The colored surface is the fit to two Gaussian functions (eqs S1–S5). (D and E)  $T$  dependence of the two Gaussian components of  $P(N_{fs}, T)$  in the (D) side and (E) top views. One Gaussian component located at  $N_{fs} \approx 4$  corresponds to LFTS, whereas the other one at  $N_{fs} \approx 5$  corresponds to DNLS, in agreement with the snapshot in (A). The fraction of the two Gaussian components is consistent with the fraction determined by the  $\zeta$  distribution in (B) and the theoretical two-state model (eq S12).

defined by local structures around a central molecule and are characterized by low and high local symmetry, energy, density, and entropy, respectively. Correspondingly, Errington and Debenedetti<sup>16</sup> introduced orientational and translational order parameters and discussed their relations to water's anomalies in model water. Here, we note that liquid water may have a second critical point associated with the liquid–liquid transition between low-density (LDL) and high-density liquids (HDL), which was discovered<sup>17</sup> and firmly confirmed<sup>18,19</sup> in model waters by numerical simulations. It is also suggested<sup>20</sup> that these two liquids may be linked to two forms of amorphous ices discovered experimentally. (See ref 21 for a review.) In the one-phase regime of water far from the second critical point (if it exists), the local structures can have only short coherence lengths. We stress that LDL and HDL are the macroscopic phases of water that can exist only below the second critical point, so it is not appropriate to regard liquid water as a mixture of LDL and HDL, which is widely used in the literature. (2) Reflecting the presence of the two states, the distribution of a proper structural descriptor should have a bimodal distribution composed of two distinct functions (not necessarily two delta functions; note that there is no unique configuration for each state under thermal fluctuations). (3) The two-state model effectively transforms to a continuum-like model at high temperatures/high pressures where there exists only the  $\rho$  state because the ordered  $S$  structure can hardly survive due to the entropy/volume penalties. (4) The  $T, P$

dependence of the fraction of the two types of local structures should obey the thermodynamic two-state equations.<sup>15</sup> (5) The existence of a second critical point is a sufficient but not necessary condition for the two-state model.

**Evidence for the Coexistence of Two Types of Local Structures in the Coordination Number Distribution.** To characterize the translational order in the second shell, Russo and Tanaka<sup>22</sup> have introduced a microscopic structural descriptor  $\zeta$  measuring the difference in the distance to the central water molecule from the nearest non-H-bonded neighbor and that from the farthest H-bonded one. Recently we have shown that we can clearly detect two types of local structures by  $\zeta$ , and we have also confirmed the above five features on a microscopic level by computer simulations of several popular water models.<sup>23–25</sup> Evidence for the coexistence of two types of local structures has also been found by other structural descriptors in various water models.<sup>26–34</sup> These studies have clearly indicated that water is a dynamic mixture of the two states<sup>14,15,22,23,25,31,35–40</sup>—the  $S$  state [locally favored tetrahedral structure (LFTS)] and the  $\rho$  state [disordered normal-liquid structure (DNLS)]. The former stabilized by four H-bonds has lower symmetry, density, energy, and entropy than the latter. A typical snapshot of LFTS and DNLS is shown in Figure 1A. We have also found that the fraction  $s$  of the LFTS, serving as an order parameter characterizing the degree of structural ordering, changes with temperature  $T$  and pressure  $P$ , obeying the prediction of the

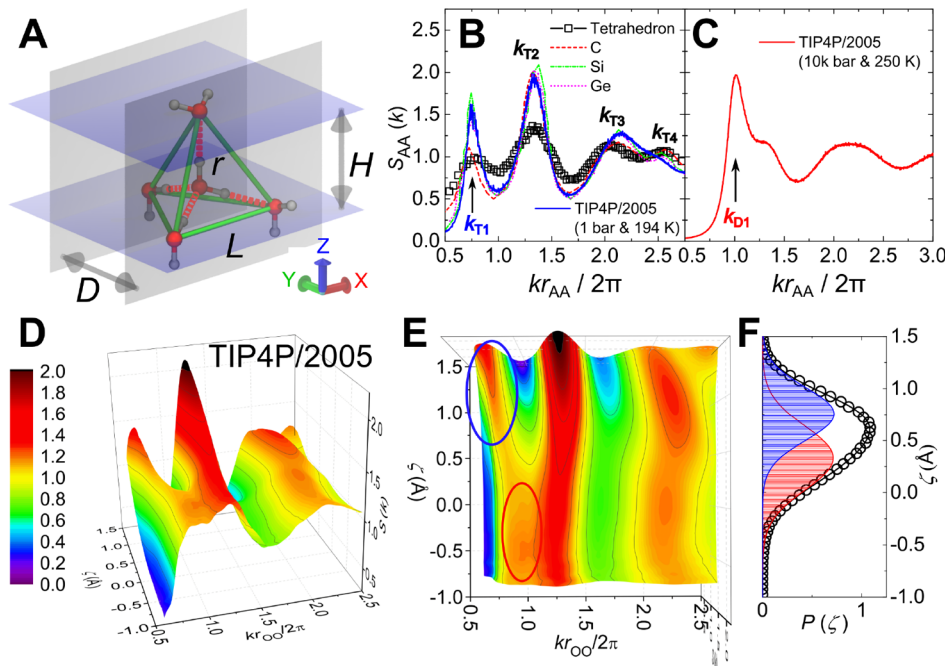


**Figure 2.** Structural bimodality in the structure factor of liquid water. (A) Schematic representation of a regular tetrahedron formed by five water molecules with the nearest O–O distance  $r = r_{\text{OO}}$ , height  $H$ , width  $D$ , and edge length  $L$ . (B) O–O partial structure factor  $S_{\text{AA}}(k)$  ( $\text{AA} = \text{OO}$ ) of a regular tetrahedron (formed by five oxygen atoms) and simulated TIP4P/2005 liquid water at 1 bar, 194 K, and  $0.9353 \text{ g cm}^{-3}$ , together with the structure factor of typical amorphous tetrahedral materials C,<sup>44</sup> Si,<sup>45</sup> and Ge.<sup>46</sup> Deeply supercooled liquid water clearly shows four characteristic peaks ( $k_{Ti}$  ( $i = 1–4$ )) common to tetrahedral materials. The peak position of FSDP,  $k_{T1} = kr_{\text{OO}}/2\pi \simeq 3/4$ , indicated by the arrow corresponds to the height  $H$  of an LFTS.<sup>42</sup> (C) O–O partial structure factor of TIPSP/2005 water at 10 000 bar, 250 K, and  $1.267 \text{ g cm}^{-3}$ . (See Figure S11 for the results of real and TIPSP water.) It shows a characteristic peak of normal disordered systems at  $k_{D1} = kr_{\text{OO}}/2\pi \simeq 1$  (see the arrow). (D and E)  $\zeta$ -dependent O–O partial structure factor  $S(k, \zeta)$  of TIP4P/2005 water at 1 bar and 240 K, calculated by Debye's scattering equation (eq 3), in (D) side and (E) top views. (See Figure S8 for TIPSP and ST2 models.) The characteristic peaks,  $k_{T1}$  and  $k_{D1}$ , are highlighted by blue and red circles, respectively. (F) The distribution of  $\zeta$  shows two Gaussian components corresponding to LFTS (blue shade) and DNLS (red shade) respectively. The wavenumbers in B, C, D, and E are scaled by nearest-neighbor distance  $r_{\text{AA}}$  for all cases (A = C, Si, Ge, and O in water).

thermodynamic two-state model.<sup>14,15,22–25</sup> These results provide strong computational support for the two-state model.

The shape of the distribution function of a microscopic physical quantity is a key to judging which of the mixture and continuum models is relevant because the former predicts a bimodal distribution at a certain range of  $T$  and  $P$  while the latter always predicts a unimodal distribution. Our structural descriptor  $\zeta$  clearly shows the bimodality (Figure S5). Then, a key question is whether a quantity directly related to local density shows such bimodality. The answer is yes. We show the distribution  $P(N_{\text{fs}})$  of the coordination number  $N_{\text{fs}}$  for TIPSP/2005 water in Figure 1B. We note that  $N_{\text{fs}}$  is the number of water molecules in the spherical first-shell volume  $V_{\text{fs}}$  of radius  $3.5 \text{ \AA}$  and thus is proportional to the local number density,  $N_{\text{fs}}/V_{\text{fs}}$ . (See Section 2 in the Supporting Information (SI) for the relevance of this estimation of local density.) We find that both  $P(N_{\text{fs}})$  and  $P(\zeta)$  can be properly characterized by two Gaussian functions (SI Section 3) with the same fraction  $s$  (Figure 1B), following the prediction of the thermodynamic two-state model (Figure 1C–E and Figures S2 and S3). This clearly indicates the anticorrelation between  $\zeta$  and local density (feature 1 above). This result strongly contradicts the prediction of the continuum models that  $P(N_{\text{fs}})$  should be unimodally Gaussian, which is the case for simple liquids such as Lennard-Jones liquids (Figure S1). We note that under substantial thermal fluctuations the two Gaussian peaks may become broader than their separation, giving rise to a broad non-Gaussian peak instead of two distinct peaks. From

Figures 1, S2, and S3, we can see that  $P(N_{\text{fs}})$  exhibits a unimodal (single Gaussian) distribution at very high  $T$  as simple liquids do but transforms to a bimodal one (composed of two Gaussians) upon cooling for all three water models. This clearly indicates the failure of continuum models and supports the two-state model (features 1–4 above).

It has sometimes been argued that the unimodal Gaussian distribution of density fluctuations is a signature against mixture models. However, we point out that this is not the case: under thermal fluctuations, any thermodynamic order parameters, e.g., density  $\rho$  and local structural order  $s$ , should have unimodal Gaussian distributions because the free energy of a system,  $f(\rho, s)$ , can be expressed by quadratic terms in the one-phase homogeneous region, e.g., ref 13. Although theoretically obvious, we can confirm it from the fact that the macroscopic density distributions in liquid water and other single- or two-component liquids commonly show Gaussian distributions (see the results of Lennard-Jones (LJ) liquid,  $\text{SiO}_2$ , and  $\text{Cu}_{64}\text{Zr}_{36}$  in Figure S4), irrespective of whether the local density distribution is unimodal or bimodal (unimodal for an LJ liquid but bimodal for  $\text{H}_2\text{O}$ ,  $\text{SiO}_2$ , and  $\text{Cu}_{64}\text{Zr}_{36}$ ). The same is applied for the distribution of another macroscopic order parameter  $s$  (estimated from  $\zeta$ ):  $P(s)$  has a unimodal Gaussian distribution, even when the underlying microscopic structural descriptor  $\zeta$  has a bimodal distribution composed of two Gaussians (Figure S5). This difference between macroscopic and microscopic distributions clearly indicates that the

bimodal structural ordering in liquid water is highly localized, in agreement with feature 1 mentioned above.

So far, we show that computer simulations of classical water models allow us to access the distributions of  $\zeta$  and  $N_{\text{fs}}$  directly and provide strong evidence for the presence of the two types of local structures. Unfortunately, however, we cannot access such microscopic molecular-level information by experiments, so an experimentally accessible structural descriptor is highly desirable for closing a long-standing debate on the structure of liquid water.

**Evidence for the Coexistence of Two Types of Local Structures in the Scattering Function.** The most powerful experimental methods used to access the local structures of materials are X-ray and neutron scattering, by which we can measure the structure factor, i.e., the density–density correlation in reciprocal space

$$S(\mathbf{k}) = \frac{1}{N} \langle \rho_{\mathbf{k}} \rho_{-\mathbf{k}} \rangle \quad (1)$$

where  $\langle \dots \rangle$  denotes the ensemble average,  $N$  is the number of particles,  $\rho_{\mathbf{k}} = \sum_{i=1}^N \exp(-i\mathbf{k} \cdot \mathbf{r}_i)$  is the number density,  $\mathbf{r}_i$  is the position vector of particle  $i$ , and  $\mathbf{k}$  is the wave vector. In a crystal, the density  $\rho_{\mathbf{k}}$  has components only at particular wave vectors  $\mathbf{k}$  because of the periodic arrangement of particles, leading to sharp diffraction spots at those wave vectors in the structure factor. These spots provide a complete description of a crystal structure. On the other hand, liquids and amorphous solids do not possess long-range translational order, and as a result, only broad isotropic amorphous halos are usually observed, which makes their structural characterization extremely difficult. This has also been the case for liquid water. So far, no clear evidence of the coexistence of two types of local structures has been detected in  $S(k)$  ( $k = |\mathbf{k}|$ ), which has been the main cause of continuous doubt in the two-state model. In this article, however, we report a new analysis of  $S(k)$  focusing on the first few peaks, which provides direct experimental evidence for the coexistence of the two types of local structures and thus supports the two-state model.

To do so, we focus on the lowest-wavenumber peak in liquid water. In simple liquids such as hard spheres and LJ liquids, the first diffraction peak usually appears at wavenumber  $\hat{k}/2\pi \simeq 1$  corresponding to the average nearest-neighbor distance  $\hat{r}$  or the average interparticle distance. However, it has been reported that  $S(k)$  of a wide class of materials has a peak at a lower wavenumber whose corresponding length is longer than the average nearest-neighbor distance.<sup>41</sup> Such a peak has been widely observed in so-called tetrahedral liquids such as SiO<sub>2</sub>, GeO<sub>2</sub>, BeF<sub>2</sub>, Si, Ge, and C and is widely known as the first sharp diffraction peak (FSDP).<sup>42</sup> The emergence of FSDP has been considered to be a signature of intermediate-range structural ordering in liquids and amorphous states. Recently we have discovered<sup>42</sup> that FSDP of these liquids originates from the scattering from the density wave characteristic of a tetrahedral unit in LFTS (formed by five atoms/molecules), which is the fundamental structural motif of tetrahedral materials. More precisely, a density wave whose wave vector corresponds to the height  $H$  of the tetrahedral structure (e.g., along the Z direction in Figure 2A) generates a sharp diffraction peak specifically at  $k_{T1} = \hat{k}/2\pi \simeq 3/4$  (i.e., the FSDP). We note that this interpretation provides a microscopic explanation of the interesting finding that a decrease in the patch size increases the network peak (FSDP in our

terminology) in tetrahedral patchy colloids.<sup>43</sup> A tetrahedral unit produces four peaks in the range of  $0.5 \leq \hat{k}/2\pi \leq 3.0$  with peak wave numbers labeled as  $k_{Ti}$  ( $i = 1–4$ ) from low to high  $\hat{k}$ <sup>42</sup> (Figure 2B). If the two types of local structures revealed by  $\zeta$  for water models are also relevant to real water, then there should be the corresponding distinct signatures in the experimentally measured structure factor. Such a signature is indeed seen from the locations of the first diffraction peak in the structure factor of low- $T$  and high- $P$  water (Figure S6). We can see a more distinct signature in simulated model waters, for which we can access both much lower temperatures (predominantly composed of LFTS) and higher pressures (predominantly composed of DNLS) than for experiments, without suffering from ice crystallization. Figure 2B,C shows the O–O partial structure factor of TIP4P/2005 water at low  $T$  (LFTS-dominant) and high  $P$  (DNLS-dominant), respectively, together with those of typical amorphous tetrahedral materials C, Si, and Ge. We can clearly see that low- $T$  water has a structure factor very similar to that of typical amorphous tetrahedral materials, and its FSDP is exactly located at  $k_{T1} = \hat{k}/2\pi \simeq 3/4$ , as expected.<sup>42</sup> On the other hand, high- $P$  water has its first diffraction peak at  $k_{D1} = \hat{k}/2\pi \simeq 1$ , as simple liquids do, reflecting its (partially) disordered nature. In the two-state regime lying between the two extreme conditions, where LFTS and DNLS coexist with comparable populations, distinct signatures from the two types of local structures are expected to appear in the structure factor of liquid water.

To reveal local structural characteristics in the wavenumber space, we employ what is called the Debye scattering function (Figure S7)<sup>47</sup>

$$S(k) = 1 + \frac{1}{N} \sum_{i=1}^N \sum_{j \neq i}^N \frac{\sin(kr_{ij})}{kr_{ij}} W(r_{ij}) \quad (2)$$

where  $W(r_{ij}) = \frac{\sin(\pi r_{ij}/r_c)}{\pi r_{ij}/r_c}$  is the window function,<sup>48</sup>  $r_{ij}$  is the distance between atoms  $i$  and  $j$ , and  $r_c$  is a cutoff distance. The Debye scattering function allows for a local structural characterization by the molecular structure factor  $S_i(k) = 1 + \sum_{j \neq i}^N \frac{\sin(kr_{ij})}{kr_{ij}} W(r_{ij})$ . Then, the correlation between molecular structure factor  $S_i(k)$  and local structure descriptor  $\zeta$  can be evaluated by the  $\zeta$ -dependent structure factor on the firm theoretical basis:

$$S(k, \zeta) = \frac{\sum_i^N S_i(k) \delta(\zeta - \zeta(i))}{\sum_i^N \delta(\zeta - \zeta(i))} \quad (3)$$

Figure 2D,E shows the  $\zeta$ -dependent O–O partial structure factor  $S(k, \zeta)$  of TIP4P/2005 water at 1 bar and 240 K, where water has an equal amount of LFTS and DNLS (or  $s = 1/2$ ). We refer to this particular temperature as the Schottky temperature<sup>25</sup> and denote it as  $T_{s=1/2}$ . Strikingly, we can see two distinct peaks at  $k_{T1}$  and  $k_{D1}$  in different  $\zeta$  domains, which are nicely characterized by the two Gaussian components in the distribution of  $\zeta$ . Thus, we may conclude that the two peaks at  $k_{T1}$  and  $k_{D1}$  in the structure factor should correspond to LFTS and DNLS, respectively (Figure 2E,F). We have also confirmed the same feature for TIPSP and ST2 water (Figure S8). Together with the bimodality of structural descriptor  $\zeta$  and coordination number  $N_{\text{fs}}$ , this result further supports the two-state model. We emphasize that our finding indicates that

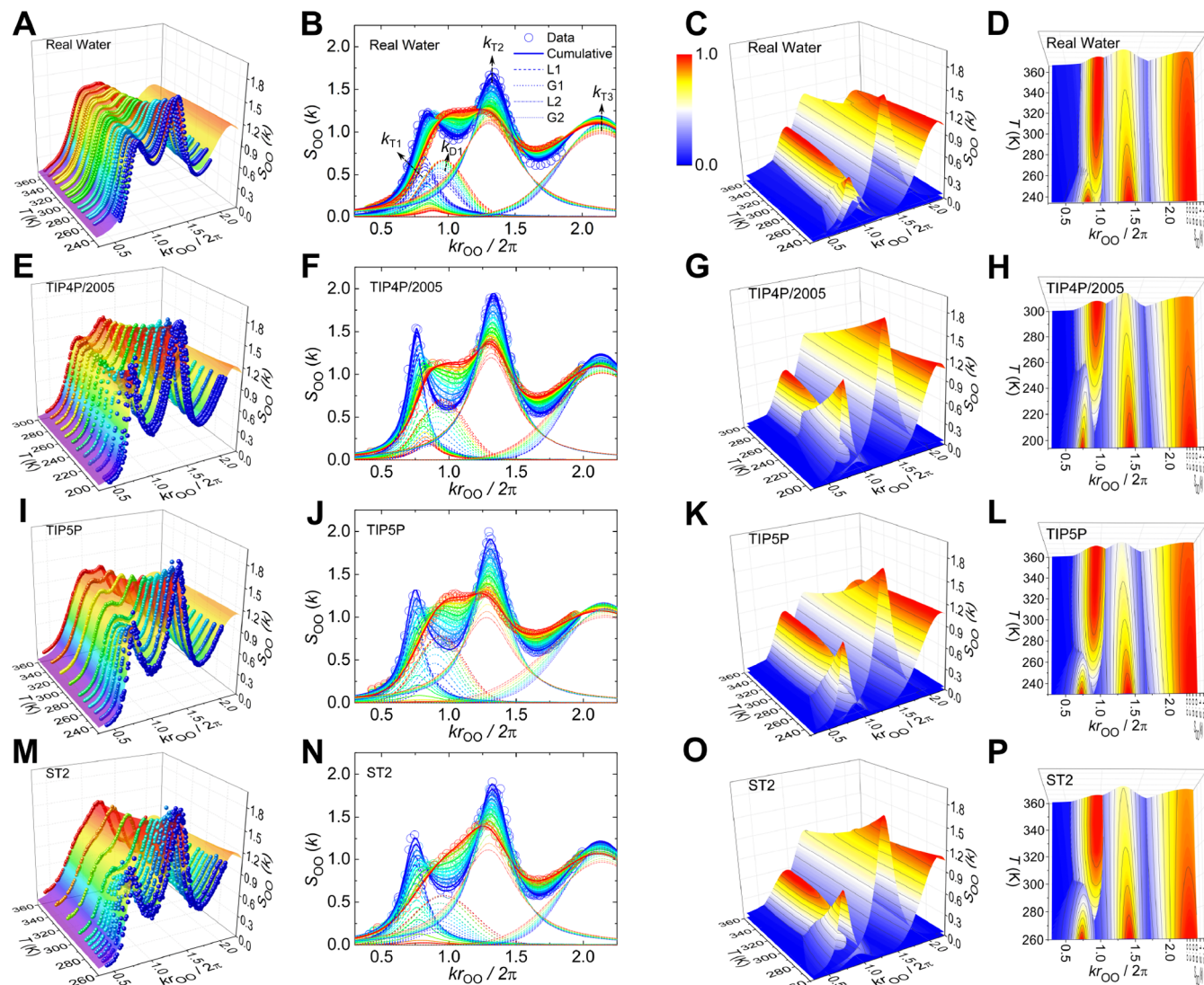


**Figure 3.** Analysis of O–O partial structure factors of real water and model waters at ambient pressure. (A–D) X-ray scattering data of real water.<sup>54,55</sup> (E–H) TIP4P/2005 model. (I–L) TIP5P model. (M–P) ST2 model. The O–O partial structure factors are shown by spheres in 3D plots (A, E, I, and M) and circles in 2D plots (B, F, J, and N) with more blue and red colors for lower and higher temperatures, respectively. The colored surfaces in (A, E, I, and M) are the fits of our model (two Lorentzian ( $L_1 + L_2$ ) and two Gaussian ( $G_1 + G_2$ ) functions; see eq S6) to the structure factors. In (B, F, J, and N), four characteristic peaks obtained from the fit are displayed by broken lines and assigned as indicated by the arrows in (B). The colored surfaces in the right two columns show the temperature dependencies of the four characteristic peaks from the fits in the side view (C, G, K, and O) and the top view (D, H, L, and P). The color bar is shown in (C), and the number in it denotes the ratio of the peak height to the maximum height of each peak over the temperature and wavenumber ranges shown in each image. The wavenumber is scaled by nearest-neighbor O–O distance  $r_{\text{OO}}$ .

we can now access the two-state signature experimentally by analyzing the structure factor of real water.

In the text above, we introduce the Schottky temperature. The Schottky temperature as a function of pressure constitutes a line of maximal two-state fluctuations, which we call the Schottky line. We introduce this new terminology besides the popular Widom line<sup>49</sup> since this line comes from the two-state features and does not require criticality. The Widom line is often defined as the line of maximal compressibility. However, a thermodynamic quantity such as compressibility is generally composed of the normal background part and the anomalous part. Thus, the location of maximal compressibility is affected by the background part. This means that the Widom line defined in this way should deviate from the Schottky line, and its deviation should increase with an increase in the distance

from the critical point. If we define the Widom line as a line of maximal critical fluctuations, then the Schottky and Widom lines coincide with each other as long as the critical fluctuations exist.

Unfortunately, however, because the  $k_{\text{T}1}$  and  $k_{\text{D}1}$  peaks are close to each other, they are heavily overlapped under substantial thermal fluctuations, which makes a clear separation difficult. This difficulty is a source of long-standing controversy. We note that the  $k_{\text{T}1}$  and  $k_{\text{D}1}$  peaks also exist in low-density amorphous (LDA) and high-density amorphous ice (HDA), respectively, and they are well separated from each other at 77 K due to the significant suppression of thermal fluctuations at low temperature (Figure S9).<sup>50–53</sup> Thanks to the strong two-state nature in liquid silica, a tetrahedral liquid structurally similar to water,<sup>23</sup> and large scattering cross

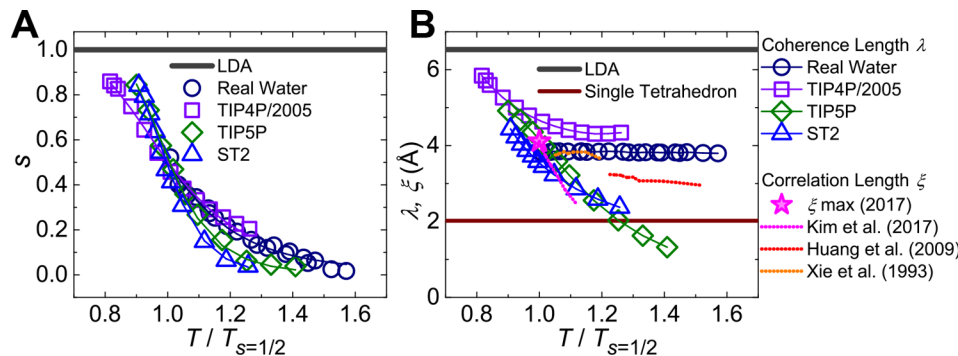


**Figure 4.** Degree and range of local tetrahedral ordering in liquid water at ambient pressure. (A) The fraction  $s$  of LFTS as a measure of the degree of local tetrahedral ordering monotonically increases upon cooling. The horizontal black line indicates the upper limit of tetrahedral ordering in liquid water. (B) The coherence length  $\lambda$  of FSDP as a measure of the range of local tetrahedral ordering monotonically increases with decreasing temperature. Here the coherence length  $\lambda$  is defined as the inverse of the half-width  $\Gamma_{T_1}$  of FSDP:  $\lambda = 1/\Gamma_{T_1}$ . The high- and low-temperature limits of the coherence length from a single tetrahedron and LDA ice<sup>53</sup> are shown by a horizontal wine-red and a black line, respectively (Figure S15). The correlation lengths determined by the Ornstein-Zernike analysis of small-angle X-ray scattering data (typically  $k < 0.5 \text{ \AA}^{-1}$ ) by different groups<sup>57–59</sup> are shown by dotted lines. The maximum correlation length of  $\xi \approx 4.1 \text{ \AA}$  at  $T_{s=1/2} = 229.2 \text{ K}$  estimated from recent small-angle X-ray scattering measurements of liquid water droplets<sup>59</sup> is shown by the magenta star symbol.

sections of the atoms, we recently found that the apparent first diffraction peak in the Si–Si partial structure factor of silica is indeed a doublet: a Lorentzian peak at  $k_{T_1}$  and a Gaussian peak at  $k_{D_1}$  are necessary to describe the apparent first diffraction peak properly. Moreover, the integrated intensity of the  $k_{T_1}$  component is proportional to the fraction  $s$  of LFTS, which is determined independently from a microscopic structural descriptor  $z$ ,<sup>23</sup> namely, it obeys the prediction of the thermodynamic two-state model.<sup>42</sup>

Recent progress of X-ray scattering techniques enables us to measure the structure factors of liquid water with high accuracy down to 234.8 K,<sup>54–56</sup> which makes a detailed structural analysis possible even for real water, as for silica. Here we analyze the O–O partial structure factors of real water as well as TIP4P/2005, TIP5P, and ST2 waters by using four peak functions for fitting (Figure 3). Indeed, we find that the apparent first diffraction peak in the O–O partial structure factors of real water as well as model waters can be nicely described by the sum of a Lorentzian ( $L_1$ ,  $k_{T_1}$  peak) and a Gaussian ( $G_1$ ,  $k_{D_1}$  peak) over a wide temperature range (Figure 3 and Figure S12). We call this the scheme II fitting scheme (SI Section 4). In particular, the Lorentzian and Gaussian functions have peaks at  $k_{T_1} = kr_{OO}/2\pi \approx 3/4$  and  $k_{D_1} = kr_{OO}/2\pi \approx 1$ , corresponding to LFTS and DNLS, respectively, in agreement with the above-mentioned silica case and the Debye scattering function shown in Figure 2. The integrated intensity of the Lorentzian peak follows the two-state model and agrees well with the fraction of LFTS,  $s$ , determined independently by  $\zeta$  and  $N_{fs}$ . Here, we note that the Lorentzian and Gaussian shapes reflect the different natures of the two types of local structures: LFTS has unique localized (spatially decaying) tetrahedral order, whereas DNLS intrinsically has disordered local environments with substantial random fluctuations. The presence of the bimodality in the experimental structure factor of liquid water (Figure 3), as well as in  $\zeta^{22–25}$  and  $N_{fs}$ , together with their interconsistency, unambiguously shows the existence of the two types of local structures (LFTS and DNLS) in liquid water and thus supports the two-state description of liquid water.

We have shown in Figures S2 and S3 that the distribution of coordination number in liquid water obeys a Gaussian distribution at high temperature. Similarly, we find that at

high  $T$ , only one Gaussian function is enough to accurately describe the apparent first diffraction peak in the experimental and simulated O–O structure factors. We call this the scheme I fitting scheme. One might think that scheme I might work at any temperature, which is expected for continuum models. Thus, to rationalize the relevance of scheme II at low  $T$  or to confirm the bimodality of the apparent first diffraction peak in an unambiguous manner, we show in Figure S13 the difference in the mean squared residual, which measures the deviation of the fit from the data between schemes I and II as a function of scaled temperature  $T/T_{s=1/2}$ . We can clearly see a tendency common to both real water and simulated model waters: at temperatures above  $\sim 1.15T_{s=1/2}$ , a single Gaussian (scheme I) can describe the apparent first diffraction peak in the structure factor equally well as a Gaussian plus a Lorentzian function (scheme II). Below  $\sim 1.15T_{s=1/2}$ , on the other hand, scheme I starts to seriously fail in describing the data, reflecting the rapid growth of the fraction of LFTS below that temperature. The failure of scheme I at low temperatures not only supports the emergence of the bimodality in the apparent first diffraction peak there but also explains why the two-state feature can hardly be observed in liquid water under ambient conditions.<sup>60–62</sup>

**Degree and Range of Local Structural Ordering.** Moreover, our two-state description (scheme II) of the structure factor provides direct experimental access to the degree and range of local structural ordering in real water. The fraction  $s$  of LFTS, which is proportional to the integrated intensity of FSDP at  $k_{T_1}$ , increases rapidly toward the LDA limit ( $s \approx 1$ ) upon cooling, as shown in Figure 4A. The increase is faster for TIP5P and ST2 water than for TIP4P/2005 and the real water, indicating the overstructured tendency in the former two models. In the two-state language, TIP5P and ST2 models overestimate the energy gain and entropy loss upon the formation of LFTS, as shown by the two-state-model parameters in Table 1.

Figure 4B shows the increase in the coherence length estimated from the width of FSDP upon cooling. Below  $T_{s=1/2}$ , the coherence lengths estimated from the experimental and simulated structure factors increase and converge toward the  $s \rightarrow 1$  (LDA) limit upon cooling. Above  $T_{s=1/2}$ , on the other hand, the fraction of LFTS, i.e., the integrated intensity of

**Table 1.** Two-State Parameters for Real Water and Model Waters

	real water	TIP4P/2005	TIPSP	ST2
$\Delta E$ (K)	-1929.0	-1802.0	-3355.9	-4612.5
$\Delta\sigma$	-8.2845	-7.5779	-13.134	-16.106
$T_{s=1/2}$	232.85	237.80	255.51	286.39

FSDP, is rather small, and thus the data suffer from significant uncertainty. In any case, the coherence length is very short, bounded between  $\sim 2$  Å of a single tetrahedron and  $\sim 6.5$  Å of LDA ice (details in Figure S15), in agreement with the previous measurements of structural correlation length<sup>57–59</sup> in real water and dynamic correlation length in TIPSP water.<sup>25</sup> The short length scales confirm the feature 1 of our two-state model in which structural ordering takes place only locally, which suggests little influence of the criticality on the behavior of liquid water at ambient pressure.

## CONCLUSIONS

We show the first clear numerical evidence in the structure factor for the dynamical coexistence of the two types of local structures, LFTS and DNLS, supporting the two-state description of liquid water. This conclusion is also supported by the existing experimental data. We reveal that liquid water exhibits the so-called FSDP in the structure factor as other tetrahedral liquids do. The FSDP provides crucial information on the fraction of LFTS: the degree of structural ordering (the order parameter of the two-state model (eq S12)) and its coherence length (the range of structural ordering). We hope that these findings will contribute to the convergence of long-standing debates on the structure of water.

## ASSOCIATED CONTENT

### Supporting Information

The Supporting Information is available free of charge at <https://pubs.acs.org/doi/10.1021/jacs.9b11211>.

Simulation details, characterization of local density, fitting formula for the coordination number distribution, and fitting formula for the structure factor ([PDF](#))

## AUTHOR INFORMATION

### Corresponding Author

Hajime Tanaka — Institute of Industrial Science, University of Tokyo, Tokyo 153-8505, Japan;  orcid.org/0000-0002-4444-1890; Email: [tanaka@iis.u-tokyo.ac.jp](mailto:tanaka@iis.u-tokyo.ac.jp)

### Author

Rui Shi — Institute of Industrial Science, University of Tokyo, Tokyo 153-8505, Japan

Complete contact information is available at: <https://pubs.acs.org/10.1021/jacs.9b11211>

### Notes

The authors declare no competing financial interest.

## ACKNOWLEDGMENTS

The authors are grateful to R. Evans for helpful discussions and A. Nilsson for providing us with the latest X-ray scattering data of liquid water (ref 55). This study was partially supported by Scientific Research (A) and Specially Promoted Research (KAKENHI grants nos. JP18H03675 and JP25000002,

respectively) from the Japan Society for the Promotion of Science (JSPS) and the Mitsubishi Foundation.

## REFERENCES

- (1) Speedy, R. J.; Angell, C. A. Isothermal compressibility of supercooled water and evidence for a thermodynamic singularity at  $-45^{\circ}\text{C}$ . *J. Chem. Phys.* **1976**, *65*, 851.
- (2) Angell, C. Water II is a "strong" liquid. *J. Phys. Chem.* **1993**, *97*, 6339–6341.
- (3) Ito, K.; Moynihan, C. T.; Angell, C. A. Thermodynamic determination of fragility in liquids and a fragile-to-strong liquid transition in water. *Nature* **1999**, *398*, 492–495.
- (4) Angell, C. A. Supercooled water. *Annu. Rev. Phys. Chem.* **1983**, *34*, 593–630.
- (5) Debenedetti, P. G. Supercooled and glassy water. *J. Phys.: Condens. Matter* **2003**, *15*, R1669.
- (6) Gallo, P.; Amann-Winkel, K.; Angell, C. A.; Anisimov, M. A.; Caupin, F.; Chakravarty, C.; Lascaris, E.; Loerting, T.; Panagiotopoulos, A. Z.; Russo, J.; Sellberg, J. A.; Stanley, H. E.; Tanaka, H.; Vega, C.; Xu, L.; Pettersson, L. G. M. Water: A tale of two liquids. *Chem. Rev.* **2016**, *116*, 7463–7500.
- (7) Narten, A. H.; Levy, H. Observed diffraction pattern and proposed models of liquid water. *Science* **1969**, *165*, 447–454.
- (8) Eisenberg, D. S.; Kauzmann, W. *The Structure and Properties of Water*; Oxford University Press: Oxford, 2005.
- (9) Handle, P. H.; Loerting, T.; Sciortino, F. Supercooled and glassy water: Metastable liquid (s), amorphous solid (s), and a no-man's land. *Proc. Natl. Acad. Sci. U. S. A.* **2017**, *114*, 13336.
- (10) Röntgen, W. C. Ueber die Constitution des flüssigen Wassers. *Ann. Phys.* **1892**, *281*, 91–97.
- (11) Pauling, L. The Structure of Water. In *Hydrogen Bonding*; Hadži, D., Ed.; Pergamon Press: New York, 1959; pp 1–6.
- (12) Pople, J. A. Molecular association in liquids II. A theory of the structure of water. *Proc. Royal Soc. London A* **1951**, *205*, 163–178.
- (13) Tanaka, H. Simple physical explanation of the unusual thermodynamic behavior of liquid water. *Phys. Rev. Lett.* **1998**, *80*, 5750.
- (14) Tanaka, H. Simple physical model of liquid water. *J. Chem. Phys.* **2000**, *112*, 799–809.
- (15) Tanaka, H. Bond orientational order in liquids: Towards a unified description of water-like anomalies, liquid-liquid transition, glass transition, and crystallization. *Eur. Phys. J. E: Soft Matter Biol. Phys.* **2012**, *35*, 113.
- (16) Errington, J. R.; Debenedetti, P. G. Relationship between structural order and the anomalies of liquid water. *Nature* **2001**, *409*, 318–321.
- (17) Poole, P. H.; Sciortino, F.; Essmann, U.; Stanley, H. E. Phase behaviour of metastable water. *Nature* **1992**, *360*, 324.
- (18) Palmer, J. C.; Martelli, F.; Liu, Y.; Car, R.; Panagiotopoulos, A. Z.; Debenedetti, P. G. Metastable liquid-liquid transition in a molecular model of water. *Nature* **2014**, *510*, 385–388.
- (19) Palmer, J. C.; Poole, P. H.; Sciortino, F.; Debenedetti, P. G. Advances in Computational Studies of the Liquid-liquid Transition in Water and Water-Like Models. *Chem. Rev.* **2018**, *118*, 9129–9151.
- (20) Mishima, O. Reversible first-order transition between two  $\text{H}_2\text{O}$  amorphs at  $\sim 0.2$  GPa and  $\sim 135$  K. *J. Chem. Phys.* **1994**, *100*, 5910–5912.
- (21) Mishima, O.; Stanley, H. E. The relationship between liquid, supercooled and glassy water. *Nature* **1998**, *396*, 329.
- (22) Russo, J.; Tanaka, H. Understanding water's anomalies with locally favoured structures. *Nat. Commun.* **2014**, *5*, 3556.
- (23) Shi, R.; Tanaka, H. Impact of local symmetry breaking on the physical properties of tetrahedral liquids. *Proc. Natl. Acad. Sci. U. S. A.* **2018**, *115*, 1980–1985.
- (24) Shi, R.; Tanaka, H. Microscopic structural descriptor of liquid water. *J. Chem. Phys.* **2018**, *148*, 124503.
- (25) Shi, R.; Russo, J.; Tanaka, H. Common microscopic structural origin for water's thermodynamic and dynamic anomalies. *J. Chem. Phys.* **2018**, *149*, 224502.

- (26) Appignanesi, G. A.; Fris, J. R.; Sciortino, F. Evidence of a two-state picture for supercooled water and its connections with glassy dynamics. *Eur. Phys. J. E: Soft Matter Biol. Phys.* **2009**, *29*, 305–310.
- (27) Cuthbertson, M. J.; Poole, P. H. Mixturelike behavior near a liquid-liquid phase transition in simulations of supercooled water. *Phys. Rev. Lett.* **2011**, *106*, 115706.
- (28) Accordino, S.; Fris, J. R.; Sciortino, F.; Appignanesi, G. Quantitative investigation of the two-state picture for water in the normal liquid and the supercooled regime. *Eur. Phys. J. E: Soft Matter Biol. Phys.* **2011**, *34*, 48.
- (29) Wikfeldt, K.; Nilsson, A.; Pettersson, L. G. Spatially inhomogeneous bimodal inherent structure of simulated liquid water. *Phys. Chem. Chem. Phys.* **2011**, *13*, 19918–19924.
- (30) Santra, B.; DiStasio, R. A., Jr.; Martelli, F.; Car, R. Local structure analysis in ab initio liquid water. *Mol. Phys.* **2015**, *113*, 2829–2841.
- (31) Singh, R. S.; Biddle, J. W.; Debenedetti, P. G.; Anisimov, M. A. Two-state thermodynamics and the possibility of a liquid-liquid phase transition in supercooled TIP4P/2005 water. *J. Chem. Phys.* **2016**, *144*, 144504.
- (32) Hamm, P. Markov state model of the two-state behaviour of water. *J. Chem. Phys.* **2016**, *145*, 134501.
- (33) Altabet, Y. É.; Singh, R. S.; Stillinger, F. H.; Debenedetti, P. G. Thermodynamic Anomalies in Stretched Water. *Langmuir* **2017**, *33*, 11771–11778.
- (34) Martelli, F. Unravelling the contribution of local structures to the anomalies of water: The synergistic action of several factors. *J. Chem. Phys.* **2019**, *150*, 094506.
- (35) Holten, V.; Limmer, D. T.; Molinero, V.; Anisimov, M. A. Nature of the anomalies in the supercooled liquid state of the mW model of water. *J. Chem. Phys.* **2013**, *138*, 174501.
- (36) Biddle, J. W.; Singh, R. S.; Sparano, E. M.; Ricci, F.; González, M. A.; Valeriani, C.; Abascal, J. F.; Debenedetti, P. G.; Anisimov, M. A.; Caupin, F. Two-structure thermodynamics for the TIP4P/2005 model of water covering supercooled and deeply stretched regions. *J. Chem. Phys.* **2017**, *146*, 034502.
- (37) Singh, L. P.; Issenmann, B.; Caupin, F. Pressure dependence of viscosity in supercooled water and a unified approach for thermodynamic and dynamic anomalies of water. *Proc. Natl. Acad. Sci. U. S. A.* **2017**, *114*, 4312–4317.
- (38) de Hijes, P. M.; Sanz, E.; Joly, L.; Valeriani, C.; Caupin, F. Viscosity and self-diffusion of supercooled and stretched water from molecular dynamics simulations. *J. Chem. Phys.* **2018**, *149*, 094503.
- (39) Anisimov, M. A.; Duška, M.; Caupin, F.; Amrhein, L. E.; Rosenbaum, A.; Sadus, R. J. Thermodynamics of Fluid Polyamorphism. *Phys. Rev. X* **2018**, *8*, 011004.
- (40) Caupin, F.; Anisimov, M. A. Thermodynamics of supercooled and stretched water: Unifying two-structure description and liquid-vapor spinodal. *J. Chem. Phys.* **2019**, *151*, 034503.
- (41) Elliott, S. R. Medium-range structural order in covalent amorphous solids. *Nature* **1991**, *354*, 445.
- (42) Shi, R.; Tanaka, H. Distinct signature of local tetrahedral ordering in the scattering function of covalent liquids and glasses. *Sci. Adv.* **2019**, *5*, No. eaav3194.
- (43) Saika-Voivod, I.; Smallenburg, F.; Sciortino, F. Understanding tetrahedral liquids through patchy colloids. *J. Chem. Phys.* **2013**, *139*, 234901.
- (44) Gilkes, K.; Gaskell, P.; Robertson, J. Comparison of neutron-scattering data for tetrahedral amorphous carbon with structural models. *Phys. Rev. B: Condens. Matter Mater. Phys.* **1995**, *51*, 12303.
- (45) Laaziri, K.; Kycia, S.; Roorda, S.; Chicoine, M.; Robertson, J.; Wang, J.; Moss, S. High-energy x-ray diffraction study of pure amorphous silicon. *Phys. Rev. B: Condens. Matter Mater. Phys.* **1999**, *60*, 13520.
- (46) Etherington, G.; Wright, A.; Wenzel, J.; Dore, J.; Clarke, J.; Sinclair, R. A neutron diffraction study of the structure of evaporated amorphous germanium. *J. Non-Cryst. Solids* **1982**, *48*, 265–289.
- (47) Debye, P. Zerstreuung von röntgenstrahlen. *Ann. Phys.* **1915**, *351*, 809–823.
- (48) Zhang, Y.-Y.; Niu, H.; Piccini, G.; Mendels, D.; Parrinello, M. Improving collective variables: The case of crystallization. *J. Chem. Phys.* **2019**, *150*, 094509.
- (49) Xu, L.; Kumar, P.; Buldyrev, S. V.; Chen, S.-H.; Poole, P. H.; Sciortino, F.; Stanley, H. E. Relation between the Widom line and the dynamic crossover in systems with a liquid–liquid phase transition. *Proc. Natl. Acad. Sci. U. S. A.* **2005**, *102*, 16558–16562.
- (50) Benmore, C.; Hart, R.; Mei, Q.; Price, D.; Yarger, J.; Tulk, C.; Klug, D. Intermediate range chemical ordering in amorphous and liquid water, Si, and Ge. *Phys. Rev. B: Condens. Matter Mater. Phys.* **2005**, *72*, 132201.
- (51) Bowron, D.; Finney, J.; Hallbrucker, A.; Kohl, I.; Loerting, T.; Mayer, E.; Soper, A. The local and intermediate range structures of the five amorphous ices at 80 K and ambient pressure: A Faber-Ziman and Bhatia-Thornton analysis. *J. Chem. Phys.* **2006**, *125*, 194502.
- (52) Winkel, K.; Mayer, E.; Loerting, T. Equilibrated high-density amorphous ice and its first-order transition to the low-density form. *J. Phys. Chem. B* **2011**, *115*, 14141–14148.
- (53) Mariedahl, D.; Perakis, F.; Späh, A.; Pathak, H.; Kim, K. H.; Camisasca, G.; Schlesinger, D.; Benmore, C.; Pettersson, L. G. M.; Nilsson, A.; Amann-Winkel, K. X-ray Scattering and O–O Pair-Distribution Functions of Amorphous Ices. *J. Phys. Chem. B* **2018**, *122*, 7616–7624.
- (54) Skinner, L. B.; Benmore, C.; Neufeind, J. C.; Parise, J. B. The structure of water around the compressibility minimum. *J. Chem. Phys.* **2014**, *141*, 214507.
- (55) Pathak, H.; Späh, A.; Kim, K. H.; Tsironi, I.; Mariedahl, D.; Blanco, M.; Huotari, S.; Honkimäki, V.; Nilsson, A. Intermediate range O–O correlations in supercooled water down to 235 K. *J. Chem. Phys.* **2019**, *150*, 224506.
- (56) Skinner, L. B.; Huang, C.; Schlesinger, D.; Pettersson, L. G.; Nilsson, A.; Benmore, C. J. Benchmark oxygen-oxygen pair-distribution function of ambient water from x-ray diffraction measurements with a wide Q-range. *J. Chem. Phys.* **2013**, *138*, 074506.
- (57) Xie, Y.; Ludwig, K. F., Jr.; Morales, G.; Hare, D. E.; Sorensen, C. M. Noncritical behavior of density fluctuations in supercooled water. *Phys. Rev. Lett.* **1993**, *71*, 2050.
- (58) Huang, C.; Wikfeldt, K. T.; Tokushima, T.; Nordlund, D.; Harada, Y.; Bergmann, U.; Niebuhr, M.; Weiss, T. M.; Horikawa, Y.; Leetmaa, M.; Ljungberg, M. P.; Takahashi, O.; Lenz, A.; Ojamäe, L.; Lyubartsev, A. P.; Shin, S.; Pettersson, L. G. M.; Nilsson, A. The inhomogeneous structure of water at ambient conditions. *Proc. Natl. Acad. Sci. U. S. A.* **2009**, *106*, 15214–15218.
- (59) Kim, K. H.; Späh, A.; Pathak, H.; Perakis, F.; Mariedahl, D.; Amann-Winkel, K.; Sellberg, J. A.; Lee, J. H.; Kim, S.; Park, J.; Nam, K. H.; Katayama, T.; Nilsson, A. Maxima in the thermodynamic response and correlation functions of deeply supercooled water. *Science* **2017**, *358*, 1589–1593.
- (60) Smith, J. D.; Cappa, C. D.; Wilson, K. R.; Cohen, R. C.; Geissler, P. L.; Saykally, R. J. Unified description of temperature-dependent hydrogen-bond rearrangements in liquid water. *Proc. Natl. Acad. Sci. U. S. A.* **2005**, *102*, 14171–14174.
- (61) Clark, G. N.; Hura, G. L.; Teixeira, J.; Soper, A. K.; Head-Gordon, T. Small-angle scattering and the structure of ambient liquid water. *Proc. Natl. Acad. Sci. U. S. A.* **2010**, *107*, 14003–14007.
- (62) Niskanen, J.; Fondell, M.; Sahle, C. J.; Eckert, S.; Jay, R. M.; Gilmore, K.; Pietzsch, A.; Dantz, M.; Lu, X.; McNally, D. E.; Schmitt, T.; Vaz da Cruz, V.; Kimberg, V.; Gel'mukhanov, F.; Föhlisch, A. Compatibility of quantitative X-ray spectroscopy with continuous distribution models of water at ambient conditions. *Proc. Natl. Acad. Sci. U. S. A.* **2019**, *116*, 4058–4063.